Alexandria Engineering Journal 118 (2025) 147–158

Contents lists available at ScienceDirect

Alexandria Engineering Journal

journal homepage: www.elsevier.com/locate/aej

Original article

Dual nature solutions of unsteady MHD hybrid Carbon nanotubes across expanding/contracting cylinder

Dhurgham Allaw [a,b,*], Norfifah Bachok [a,c], Norihan Md Arifin [a,c], Fadzilah Md Ali [a,c], Abderrahim Wakif [d]

[a] Institute for Mathematical Research, Universiti Putra Malaysia, 43400 UPM Serdang, Selangor Darul Ehsan, Malaysia
[b] University of Information Technology and Communications, Baghdad, Iraq
[c] Department of Mathematics, Faculty of Science, Universiti Putra Malaysia, 43400 UPM Serdang, Selangor Darul Ehsan, Malaysia
[d] Laboratory of Mechanics, Faculty of Science Aïn Chock, Hassan II University, 20000, Casablanca, Morocco

ARTICLE INFO

Keywords:
MHD
Unsteady flow
Hybrid carbon nanotubes
Stretching/ Shrinking cylinder
Duality solution

ABSTRACT

Carbon nanotubes (CNTs) have proven their value in diverse multidisciplinary applications. For this purpose, the current study sheds light on time-reliant properties of electrically conducting flow of hybrid carbon nanotubes, scenario involving joule dissipation at a permeable cylinder that can expand and shrink. To get a precise insight into numerical outcome, the unsteady governing momentum and energy equations in cylindrical coordinates rendered into pertinent ODEs via incorporating the rescaling technique, Thereafter, the rendered equations cracked numerically via a built-in function in MATLAB (BVP4C) package. Notably, the sundry parameters yield two distinct solutions in both assisting and opposing zones, so the flow separation is identified. The governing physical factors are well explored through various graphical forms with physical explanations. Graphical observations declare, that heightening the value of curvature and volume fraction parameters contributes to speed up the onset of turbulence flow, augmentation in skin friction rate is noted through unsteadiness, magnetic field, and curvature parameters. Additionally, the stability assessment clearly specifies the mathematical robustness of the first branch as time passes. This study stands out for it is an inimitable configuration that holds significant addition in optimization of modern heat transfer applications.

1. Introduction

The capability of fluids to transport heat remains as a booming research spot due to its exponential growth in industrial applications. The progression of today's industries demands reliable transmission, minimal energy losses, and a swift cooling process. Flow geometry, externally applied forces, conditions at the restricted surfaces, and thermophysical properties of nanoparticles play a direct role in the thermal regulation of the desired product. When heat transfer via an ordinary functioning medium (water, lubricants, motor oils, ethanol or glycols), becomes restricted, due to poorly conduct heat. In view of these challenges, many studies have been conducted to promote proper thermal attributes. Choi [1] discovered nanofluids in a remarkable experiment. The thermal characteristics of nanofluids are much beyond those of ordinary liquids, Nanofluids find applications in everyday life, including phase conversion exchange transfer, solar power generation, microelectronic heat transport components, cooling and heating houses, etc. A long time ago, Crane's study [2] highlighted the 2D steady flow due to extendable (stretched) plate that travel in a linear direction. Wang [3] reported a theoretical effort to expound the extended cylinder. The most two exquisite approaches that describe transportation characteristics of nanofluid are the one-phase (Tiwari–Das) model [4] and the two-phase (Buongiorno) model [5]. Tiwari [4] prime focus was on volumetric friction. Based on Buongiorno [5], Brownian motion with thermophoresis were the pivotal mechanism, with looking at concentrations of nanoparticles in mixture. A study done by Bachok et al. [6] exposed successfully dual nature via moving surface. In a similar vein, Merkin et al. [7] evaluated numerically the duality nature of a stagnant point past exponential contracting cylinder. In vertical surface, Dinarvand et al. [8] interest was in the development of a double-diffusive stagnation point of nanofluid. Sandeep and Sulochana [9] addressed many factors such as chemical reaction, suction/injection, mixed convection and heat source, involving duality stretching of micropolar fluid. Khan et al. [10] offered an analytical and numerical analysis of Jeffery–Hamel due to extendible walls, under the consequence of Soret, Dufour and viscous dissipation. Turkyilmazoglu. [11] scrutinized independently the impact of suction on a

* Corresponding author at: Institute for Mathematical Research, Universiti Putra Malaysia, 43400 UPM Serdang, Selangor Darul Ehsan, Malaysia.
E-mail address: dhurgham.ridha@uoitc.edu.iq (D. Allaw).

https://doi.org/10.1016/j.aej.2025.01.026
Received 21 August 2024; Received in revised form 30 November 2024; Accepted 7 January 2025
Available online 21 January 2025

Nomenclature

C_f	local skin friction
q_w	heat flux at the surface
s	suction/injection parameter
(u, v)	velocity component at x, r-direction $(\mathrm{m/s})$
(x, r)	cylinder coordinated (m)
A	unsteady parameter
a	radius of the cylinder
B_0	magnitude of the magnetic field strength
Ec	Eckert number
f	similarity function
k	thermal conductivity $(\mathrm{Wm^{-1}k^{-1}})$
l	characteristic length (m)
M	Magnetic parameter
Nu_x	local nusselt number
Re_x	local Reynolds number
T	temperature
t	time (s)
T_0	reference temperature (k)
T_∞	temperature far away from the surface (k)
T_w	temperature of cylinder at the plate (k)
U_∞	free stream velocity $(\mathrm{ms^{-1}})$
u_w	plate velocity
v_w	mass flux velocity $(\mathrm{ms^{-1}})$
SWCNTs	Single wall Carbon Nanotube
MWCNTs	Multi wall Carbon Nanotube
Pr	Prandtl number

Greek letters

α	eigenvalue
β	flow unsteady parameter
γ	curvature parameter
λ	extending/shrinking parameter
μ	dynamic viscosity of fluid $(\mathrm{kgm^{-1}}s^{-1})$
ϕ_1, ϕ_2	control volume fraction for SWCNTs and MWCNTs ()
ρ	fluid density $(\mathrm{kgm^{-3}})$
σ	electrical conductivity $(\mathrm{m^2s^{-1}})$
τ	dimensionless variable
θ	dimensionless temperature

Subscripts

c	critical value
f	host fluid
nf	nanofluid
HCNTs	hybrid carbon nanotubes

rotating expanding sphere.

One of the flaws of nanofluids is unable to mend all the thermophysical attributes. To beat this downside, hybrid nanofluid was prompted. Hybrid nanofluids spark enthusiasm among investigators with their improved stability and ultra-ranked thermal consequences due to synergistic effect. Hybrid nanofluid is more sophisticated to prepare, made up by blends two or more constructive characteristics of nanoparticles in a carrier fluid, applicable in a variety of solicitations in heat exchangers, cooling and heating in buildings, heat pipes, cooling for electronics, solar panels, and many more. Under the impact of thermal radiation, Zainal et al. [12] observed how Arrhenius kinetics effect hybrid nanofluid. The author's results showed that hybrid nanofluids have a better ability to transmit heat with an increase in the rate of volume fraction. Mahmood et al. [13] developed a mathematical model of $(Al_2O_3 + Cu + TiO_2/H_2O)$ over contracting/extending nonlinear sheet with including Smoluchowski temperature action. Also concluded the control volume friction of tri-hybrid improved velocity and temperature curved.

A Swedish physicist, Alfvén [14], meticulously explicates the phenomenon of MHD that generates an orthogonal resistive nature to stabilize the flow stream. The presence of such a phenomenon has a significant value owing to its capacity to retard flow separation, allowing it to fulfill particular requirements to present high-end products. Optical grafting, gastric medications, and sterilized devices are a few real-world applications that make use of MHD. By including MHD and radiation, Fayyadh et al. [15] employed scaling analysis to analyse the Sutterby stagnation point over extending plate. Their results showed that, ameliorate MHD leads to speeds up the detachment of flow. In vertical extruded surface, Mahmood et al. [16] did research on MHD stagnation region with nanoparticles aggregation. The authors noted the Nusselt number and skin friction experience an upsurge rate with the enormity of MHD. Mahabaleshwar et al. [17] conducted a study on the movement of $(Al_2O_3 + Cu/H_2O)$ via porous expanding sheet. They extracted the analytical outcomes and observed the intensity of inclined magnetic field dampens transverse and axial velocity profiles. Recently, Soomro et al. [18] adapted Buongiorno's model to reveal the stability aspect of MHD radiative Casson flow over a permeable cylinder. On the other hand, Eckert number has emerged as a focal point of study and has significant interaction with MHD fluid flow. The process of converting an electric current's energy into a thermal state through collision was clarified by James Prescott Joule in 1840. Common examples of utilization Ohmic heating are portable fan heaters, evaporation, circuit breakers, electric stoves, and toaster ovens. Abbas et al. [19] debated the impact of MHD Sutterby flow with Darcy resistance and Eckert number over stretching cylinder. Lately, a stability assessment was proffered by Wang et al. [20] based on magnetized hybrid nanofluid under the combined effects of cross-diffusion together with Joule heating.

Carbon nanotubes (CNTs) are horn-shaped cylindrical nanomaterial, formed by a thick sheet of graphene with strong bonds, belonging to fullerenes family. CNTs alienated into (MWCNTs) connote as a bundle of nested around a central hollow tube with a constantly increasing diameter (ranging from 2 to 50 nm), whereas the other form is coated by a single-atom-thick layer, denoted as (SWCNTs) with a diameter of $0.5 - 1.5$ (nm) where the length is unlimited, due to different methods of preparation. CNTs have a unique and distinct thermal conductivity not comparable with other nanoparticles due to its strength of atomic bounds. CNTs can tackle sufficient mechanical exertion without deforming nor breaking, due to outstanding tensile strength [21]. Owing to its biocompatibility, CNTs are burgeoning in nanomedicine and pharmacy, such as drug management, surgical aids, viral detection, vaccine administration, and treatment of cancer cells [22,23]. Furthermore, other distinguishing sets of traits CNTs offer: featherweight, chemical stability, rigidity, unique architecture, and high elasticity (can extend up to 20% from its original length), make them a top priority for improving the heat transfer rate. CNTs opened new avenues for designing compact nanostructures in a myriad of appliances (e.g., gadgets, composite polymer reinforcement, electrochemical analysis, bulletproof vests, hydrogen storage, and radar absorber coatings) [24,25]. Predictably, to be applicable in a new generation of flexible phones as well as in space vehicles and military fields [26,27].

In the vitro studies, Sumio Iijima [28] initiated a remarkable study and announced the discovery of the most distinctive nanostructures available today, known as MWCNTs. Two years later, another inimitable invention was carried out by presenting the most growing nanomaterial SWCNTs [29]. Waqas et al. [30] prepared a numerical calculation of carbon nanotube flow, including Darcy–Forchheimer relation and slip action via a rotating disk. To account the impact of magnetic source, Gholinia et al. [31] examined the control volume of CNTs in hybrid carrier fluid ($C_2H_6O_2-H_2O$), through a porous stretching cylinder. In another study, Muhammad et al. [32] showed that HCNTs is more efficient than SWCNTs in numerical comparison. Regarding inclined magnetic field and heat source factor via a porous medium with water-carrying CNTs was explored by Hussain and Sheremet [33]. During their research, they point out the addition of CNTs volume friction shows a positive correlation with temperature curves. To inspect the HCNTs flow over a vertically expanding plate, Duraihem et al. [34] reported the results of the impact of velocity slip and thermal stratification. In a rotating sphere with thermophoretic particle deposition, Ramesh et al. [35] looked into the nature of stagnation point of HCNTs flow, and concluded that HCNTs offer superior thermal performance when compared to single counterparts. Not long ago, Rafique et al. [36] conducted a 3D numerical analysis of MHD with suspended CNTs including Joule heating. In their work noted that Eckert number leads to thermal boundary layer goes up. More investigations with distinct scenarios regarding carbon nanotubes are mentioned here [37–42].

Unsteadiness occurs due to various factors in real-world situations. Including unsteadiness features adds a certain complexity to the flow. Most natural (artificial) flow experiences different scenarios, such as start-up or shut-down (transitory demeanour) and periodic movement. Nozzle flows, hydrofoil flutter, bonnet of cars, sediment transport in rivers, and processing of materials geophysical are all pragmatic applications that involve time-varying flow [43,44]. Bhattacharyya [45] worked independently on the nature of double solutions of unsteady stagnation vicinity with contracting or extending plate. Veera Krishna et al. [46–48] showcased the time-fluctuation attribute of a MHD flow of (nanofluid, elastico-viscous, and Jeffreys fluids) over different configurations, and extracted the analytical outcomes of engineering inquisitiveness. Suganya et al. [49] went into a complex examination to analyse the unsteady fluctuation of 3D HCNTs subject to heat absorption/generation and chemical reacting. In another research endeavour, Allaw et al. [50] conducted a thorough investigation to assess the duality behaviour of CNTs via an exponential penetrable contractable plate with the impression of slip action. Recently, Mahabaleshwar et al. [51] presented exact solutions by utilizing incomplete gamma function and tested in their work the non-unique solution of unsteady rear stagnation point, across a penetrable stretchable plate containing CNTs. More recently, Tulu et al. [52] considered in a rotating disk, the ($MWCNTs/Fe_3O4-H_2O$) of unsteady MHD flow subject to Eckert number and viscous dissipation.

1.1. Motivation

Given the growing urgency of an efficient cooling system with significant applications of flow around horizontal cylinders. Furthermore, the paucity of consideration a complex fluid dynamics behaviour (time-dependent), which acts as another piece of motivation. In a nutshell, due to the high necessity to develop a mathematical model of unsteady flow around a horizontal cylinder with extraordinary nano-material. This research considers unsteady flow of ($SWCNTs–MWCNTs/H_2O$) over a stretchable (shrinkable) cylinder surface with the presence of MHD and suction. A single-phase model introduced by (Tiwari and Das) [4] with Xue model [53] are adapted. A powerful technique (BVP4C) is attaining numerical data. Moreover, the identification of double solutions in both zones (assisting and opposing) and stability analysis presents another distinguishing aspect, allowing for the management of the flow according to certain desires. Tables and visual depictions were generated to describe physical impact and to provide other researchers and scientists with deeper insights for future studies. The authentic and unique results would be beneficial for propelling engineering design as well as for industrial processes where a huge amount of heat transport is required.

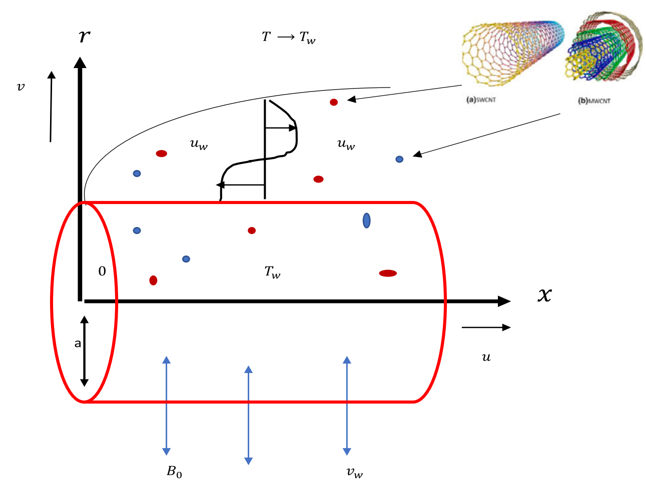

Fig. 1. The schematic diagram of fluid flow.

2. Mathematical formulation

To construct the present model, the time-varying magnetized flow is considered with tiny fragments of (SWCNTs–MWCNTs) in a permeable medium of stretching/shrinking cylinder Fig. 1. Water (H_2O) serves as host fluid. The time-dependent velocity $U_w(x,t) = u_0 x/L(1-\beta t)$ where β is the constant expansion/contraction strength. The ambient hybrid carbon nanotube temperature is referred as T_∞ and T_0 is characteristic temperature. While the temperature distribution near the surface is referred as $T_w(x,t) = T_\infty + \left(T_0(x/L)^2\right)/(1-\beta t)^2$. The current analysis is mathematically modelled under the subsequent assumptions and constraints.

- ▷ The flow is presumptively valid for laminar behaviour, time-reliant, two-dimensional, and incompressibility attributes.
- ▷ Frame coordinates of cylinder are selected in which x is marked along stretching/shrinking cylinder while r coordinate is normal to it with constant radius a,
- ▷ Hybrid carbon nanotubes created a SWCNTs–MWCNTs/ H_2O by mixing SWCNTS and MWCNTs in water. .
- ▷ An external magnetic field of uniform strength B_0 is applied perpendicular to unsteady cylinder (along the x-axis).
- ▷ The Eckert number modify the energy equation.
- ▷ The mass flux velocity for suction is $v_w(x,t) < 0$ and for injection is $v_w(x,t) > 0$ are considered in cylinder surface.

With the given assumptions and limitation, the framework of the governing equation for hybrid carbon nanotubes depicted in cylindrical coordinates stated as (based on [54–57]):

$$\frac{\partial(ru)}{\partial x} + \frac{\partial(rv)}{\partial r} = 0, \tag{1}$$

$$\frac{\partial u}{\partial t} + u\frac{\partial u}{\partial x} + v\frac{\partial u}{\partial r} = \frac{\mu_{hcnt}}{\rho_{hcnt}}\left(\frac{\partial^2 u}{\partial r^2} + \frac{1}{r}\frac{\partial u}{\partial r}\right) - \frac{\sigma_{hcnt} B_0^2 u}{\rho_{hcnt}}, \tag{2}$$

$$\frac{\partial T}{\partial t} + u\frac{\partial T}{\partial x} + v\frac{\partial T}{\partial r} = \frac{k_{hcnt}}{(\rho C_p)_{hcnt}}\left(\frac{\partial^2 T}{\partial r^2} + \frac{1}{r}\frac{\partial T}{\partial r}\right) + \frac{\sigma_{hcnt} B_0^2 u^2}{(\rho C_p)_{hcnt}}, \tag{3}$$

In the above aforesaid, u and v represents the components of velocity in x and r-direction, respectively. Apart from that, the unsteady boundary layer at the surface and far from it given as [55]:

$$\text{at } r = a \ : \quad v = v_w(r,t), u = \lambda U_w(x,t), T = T_w(x,t)$$

$$\text{as } r \to \infty : u \to 0, \quad T \to T_\infty; \tag{4}$$

Note that, ϕ_1 and ϕ_2 refer to nanoparticles of SWCNTs and MWCNTs, respectively, where, $\phi_{hcnt} = \phi_1 + \phi_2$ is the net volume concentration

Table 1
Features of host fluid and CNTs [58,59].

Physical properties	$k(Wm^{-1}K^{-1})$	$C_p(Jkg^{-1}K^{-1})$	$\rho(kgm^{-3})$	$\sigma(Sm^{-1})$	Prandtl number
H_2O 	0.613	4179	997.1	5.5×10^{-6}	6.2
SWCNTs 	6600	425	2600	4.8×10^{7}	–
MWCNTs 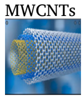	3000	796	1600	1.9×10^{-4}	–

Table 2
The correlation coefficient [37,57].

Properties	Formulations of (SWCNTs–MWCNTs/H_2O)
Dynamic viscosity	$\mu_{hcnt} = \frac{\mu_f}{(1-\phi_{hcnt})^{5/2}}$
Density	$\rho_{hcnt} = (1-\phi_2)\left[(1-\phi_1)\rho_f + \phi_1\rho_{SWCNT}\right]\phi_2\rho_{MWCNT}$
Thermal Capacity	$(\rho C_p)_{hcnt} = (1-\phi_2)\left[(1-\phi_1)(\rho C_p)_f + \phi_1(\rho C_p)_{SWCNT}\right] + \phi_2(\rho C_p)_{MWCNT}$
Thermal conductivity	$\frac{k_{hcnt}}{k_{bf}} = \left[\frac{(1-\phi_2)+2\phi_2\frac{k_{MWCNT}}{k_{MWCNT}-k_{bf}}\ln\left(\frac{k_{MWCNT}+k_{bf}}{2k_{bf}}\right)}{(1-\phi_2)+2\phi_2\frac{k_{bf}}{k_{MWCNT}-k_{bf}}\ln\left(\frac{k_{MWCNT}+k_{bf}}{2k_{bf}}\right)}\right]$
	where $\frac{k_{bf}}{k_f} = \left[\frac{(1-\phi_1)+2\phi_1\frac{k_{SWCNT}}{k_{SWCNT}-k_f}\ln\left(\frac{k_{SWCNT}+k_f}{2k_f}\right)}{(1-\phi_1)+2\phi_1\frac{k_f}{k_{SWCNT}-k_f}\ln\left(\frac{k_{SWCNT}+k_f}{2k_f}\right)}\right]$
Electrical conductivity	$\frac{\sigma_{hcnt}}{\sigma_{bf}} = \left[\frac{\sigma_{MWCNT}+2\sigma_{bf}-2\phi_2(\sigma_{bf}-\sigma_{MWCNt})}{\sigma_{MWCNT}+2\sigma_{bf}+\phi_2(\sigma_{bf}-\sigma_{MWCNT})}\right]$
	where $\frac{\sigma_{bf}}{\sigma_f} = \left[\frac{\sigma_{SWCNT}+2\sigma_f-2\phi_1(\sigma_f-\sigma_{SWCNT})}{\sigma_{SWCNT}+2\sigma_f+\phi_1(\sigma_f-\sigma_{SWCNT})}\right]$

of hybrid carbon nanotubes. Following that, Table 1 provides the characteristics of water, SWCNTs and MWCNTs. The hybrid carbon nanotubes correlation are outlined in Table 2. Herein, u and v being the corresponding velocity component in the x and r directions, μ_{hcnt}, ρ_{hcnt} are the dynamic viscosity and density of hybrid carbon nanotubes, B_0 is the uniform magnetic field, σ is an electrical conductivity. Where $(\rho C_p)_{hcnt}$ and k_{hcnt} refers to thermal capacity and thermal diffusivity of hybrid carbon nanotubes. λ is the constant stretching /shrinking parameter, where $\lambda = 0$ for static cylinder, $\lambda > 0$ for stretching and $\lambda < 0$ for shrinking. Further, now define the rescaling transformation:

$$u = \frac{u_0 x}{L(1-\beta t)} f'(\eta), v = -\frac{a}{r}\left(\frac{u_0 v_f}{L(1-\beta t)}\right)^{1/2} f(\eta),$$
$$\theta(\eta) = \frac{T-T_\infty}{T_w - T_\infty}, \eta = \left(\frac{u_0}{v_f L(1-\beta t)}\right)^{1/2}\frac{r^2-a^2}{2a} \quad (5)$$

here η similarity variables, on substituting Eq. (5) into Eqs. (2)–(4), we obtain:

$$\frac{\mu_{hcnt}/\mu_f}{\rho_{hcnt}/\rho_f}\left[2\gamma f'' + (1+2\eta\gamma)f'''\right] + f''(f - \frac{A\eta}{2}) - f'(A+f') - \frac{\sigma_{hcnt}/\sigma_f}{\rho_{hcnt}/\rho_f} M f' = 0 \quad (6)$$

$$\frac{1}{Pr}\frac{k_{hcnt}/k_f}{(\rho C_p)_{hcnt}/\rho_f C_p}\left[2\gamma\theta' + (1+2\eta\gamma)\theta''\right] + \theta'(f - A\frac{\eta}{2}) - 2\theta(A+f')$$
$$+ \frac{\sigma_{hcnt}/\sigma_f}{(\rho c_p)_{hcnt}/\rho(c_p)_f} M Ec f'^2 = 0 \quad (7)$$

Subject to:

$$f'(0) = \lambda, f(0) = S, \ \theta(0) = 1$$
$$f'(\eta) \to 0, \ \theta(\eta) \to 0 \quad \text{as } \eta \to \infty \quad (8)$$

herein, prime ($'$) refers to differentiation with respect to η and $v_w(r) = -\frac{a}{r}\left(\frac{u_0 v_f}{L(1-\beta t)}\right)^{1/2} S$ is represent mass flux velocity. Where curvature parameter represent as $\gamma = \sqrt{v_f L(1-\beta t)/u_0 a^2}$. The unsteady parameter defined as $A = \frac{\beta L}{u_0}$, when ($A < 0$) represent decelerating flow, ($A > 0$) represent accelerating flow and Prandtl number are termed by Pr= $\mu_f C_p/k_f$, Eckert number denotes as $Ec = \frac{U_w^2}{(c_p)_f(T_w(x)-T_\infty)}$. In the meanwhile, $M = \frac{\sigma_f B_0^2}{\rho_f u_0}$ is magnetic parameter applied to fluid flow. Since the magnetic Reynolds number is supposed to be small, the induced magnetic field is neglected. The significant factors of the gradients are the skin friction coefficients (shear stress) C_f and the local Nusselt number (heat transmission rate) Nu_x declared as:

$$C_f = \frac{\tau_w}{\rho_f U_w^2}, Nu_x = \frac{x q_w}{k_f(T_w - T_\infty)} \quad (9)$$

for more clarification, the values of τ_w represent the shear stress at the interface and q_w represent as the energy flux at the surface that accentuated by:

$$\tau_w = \mu_{hcnt}\left(\frac{\partial u}{\partial r}\right)_{r=0}, q_w = -k_{hcnt}\left(\frac{\partial T}{\partial r}\right)_{r=a}, \quad (10)$$

The following relation acquired through similarities variable.

$$C_f Re_x^{1/2} = \frac{\mu_{hcnt}}{\mu_f} f''(0),$$
$$Nu_x Re_x^{-1/2} = -\frac{k_{hcnt}}{k_f}\theta'(0), \quad (11)$$

In which $Re_x = u_0 x^2/v_f L(1-\beta t)$ symbolizes the local Reynolds number in x-direction.

3. Stability flow solution

In industrial processes, the analysis of stability is momentous to obtain a stable procedure for transmission heat, where it is required to detect how the nature of the system changes after applying tiny perturbation with passage of time. Stability aspects successfully implemented by Soomro et al. [18], D. Allaw et al. [50], Waini et al. [55], and Mahabaleshwar et al. [60] with considering different geometry. In this regard, we perform a thorough analysis of the stability due to constituted of dual solutions of Eqs. (6)–(7). To do this, following the endeavours of Merkin [61], firstly, consider the following:

$$u = \frac{u_0 x}{L(1-\beta t)} f'(\eta,\tau), v = -\frac{a}{r}\left(\frac{u_0 \upsilon_f}{L(1-\beta t)}\right)^{1/2} f(\eta,\tau),$$
$$\theta(\eta) = \frac{T-T_\infty}{T_w - T_\infty}, \eta = \left(\frac{u_0}{\upsilon_f L(1-\beta t)}\right)^{1/2}\frac{r^2-a^2}{2a},$$
$$\tau = \frac{u_0}{L(1-\beta t)} t \tag{12}$$

In the above context, τ alludes to a new non-dimensional time factor which is consistent with initial value problems. Next, plugging Eqs. (12) into Eqs. (2) and (3), we get:

$$\frac{\mu_{hcnt}/\mu_f}{\rho_{hcnt}/\rho_f}\left[(1+2\eta\gamma)\frac{\partial^3 f}{\partial \eta^3} + 2\gamma\frac{\partial^2 f}{\partial \eta^2}\right] - \frac{\partial^2 f}{\partial \eta^2}\left(\frac{A\eta}{2} - f\right) - \frac{\partial f}{\partial \eta}\left(A + \frac{\partial f}{\partial \eta}\right) = 0$$
$$- \frac{\partial^2 f}{\partial \eta \partial \tau}(1+\tau A) - \frac{\sigma_{hcnt}/\sigma_f}{\rho_{hcnt}/\rho_f} M \frac{\partial f}{\partial \eta} = 0, \tag{13}$$

$$\frac{1}{Pr}\frac{k_{hcnt}/k_f}{(\rho C_p)_{hcnt}/(\rho C_p)_f}\left[(1+2\eta\gamma)\frac{\partial^2 \theta}{\partial \eta^2} + 2\gamma\frac{\partial \theta}{\partial \eta}\right] + \frac{\partial \theta}{\partial \eta}(f - \frac{A\eta}{2}) - 2\theta(A + f')$$
$$- \frac{\partial \theta}{\partial \tau}(1 + A\tau)$$
$$+ \frac{\sigma_{hcnt}/\sigma_f}{(\rho c_p)_{hcnt}/(\rho c_p)_f} 2M\,Ec f_0' F' = 0, \tag{14}$$

subject to new bordered conditions:

$$f'(0,\tau) = \lambda, f(0,\tau) = s,\ \theta(0,\tau) = 1$$
$$f'(\infty,\tau) \to 0,\ \theta(\infty,\tau) \to 0. \tag{15}$$

To test the stability of dual solutions, some slight perturbation functions are considered, $f(\eta) = f_0(\eta)$, $\theta(\eta) = \theta_0(\eta)$ in the current model by using the following functions (Weidman et al. [62]):

$$f(\eta,\tau) = f_0(\eta) + e^{-\alpha\tau}F(\eta,\tau),$$
$$\theta(\eta,\tau) = \theta_0(\eta) + e^{-\alpha\tau}G(\eta,\tau), \tag{16}$$

Moreover, the symbol α is an unidentified eigenvalue that delivers an endless set of eigenvalues ($\alpha_1 < \alpha_2 < \alpha_3 < \cdots$). The mark (negative or positive) of the eigenvalue leads to dictates the stability of the outcomes. When α is positive detect a stable flow which shows a decline of disturbance with passage of time. In contrast, when α is negative at this point the flow is unstable and indicate early growth of disturbance with passage of time. Thus, by putting $\tau = 0$, leads to $F(\eta) = F_0(\eta)$ and $G(\eta) = G_0(\eta)$ are obtained. After plugging Eq. (16) into Eq. (13) and Eq. (14), we obtained linearized eigenvalue problem as follows:

$$\Rightarrow \frac{\mu_{hcnt}/\mu_f}{\rho_{hcnt}/\rho_f}[(1+2\eta\gamma)F''' + 2\gamma F''] + F''(f_0 - \frac{A\eta}{2})$$
$$- 2f_o' F' + f_0'' F + F'(\alpha - A) - \frac{\sigma_{hcnt}/\sigma_f}{\rho_{hcnt}/\rho_f} M F' = 0, \tag{17}$$

$$\Rightarrow \frac{1}{Pr}\frac{k_{hcnt}/k_f}{(\rho C_p)_{hcnt}/(\rho C_p)_f}\left[(1+2\eta\gamma)G'' + 2\gamma G'\right] + G'\left(f_0 - \frac{A\eta}{2}\right)$$
$$+ \theta_0' F - 2(\theta_0 F' + GA + G f_0') + \alpha G$$
$$+ \frac{\sigma_{hcnt}/\sigma_f}{(\rho c_p)_{hcnt}/(\rho c_p)_f} 2M\,Ec f_0' F' = 0, \tag{18}$$

owing to the transformed condition:

$$F'(0,\tau) = 0, F(0,\tau) = 0,\ G(0,\tau) = 0$$
$$F'(\infty) \to 0,\ G(\infty) \to 0. \tag{19}$$

Finally, to detect an envisaged spectrum of eigenvalues Eqs. (17)–(19), Harris et al. [63], state that for the far field boundary requirements $F'(\infty) \to 0$ must be unperturbed and swapped with a new condition $F''(0) = 1$.

4. Computational algorithm

Availing the numerical capabilities of MATLAB's (bvp4c code), the dimensionless controlling (Eqs. (6)–(8)) were numerically integrated for sundry parameters. This software solver has the wherewithal of reliability and is exploited broadly in engineering and mathematics. Even with complex geometry, bvp4c technique provides accurate numerical solutions with minor errors. A preliminary estimation is required to execute the algorithm. A proper guess will reduce the run time and divulge two distinct solutions (paired solutions). Otherwise, poor guess will face a singular Jacobian problem (warning signs appeared). To attain meticulous numerical outcomes, tolerance threshold between the two iteration is fell below 10^{-6}. The code Bvp up to fourth accuracy order is kind of sluggish and intensive for stiff issues. This well-established approach named as a continuation, was introduced by Shampine et al. [64]. In order to start this approach, Eqs. (6)–(8) converted into 1-st order approximations as below:

$$f = y(1),\ f' = y(2),\ f'' = y(3),\ \theta = y(4),\ \theta' = y(5) \tag{20}$$

So that the converted momentum Eq. (6) becomes:

$$\frac{1}{(1+2\gamma\eta)}\left[\frac{\rho_{hcnt}/\rho_f}{\mu_{hcnt}/\mu_f}\left(-y(3)(y(1) - \frac{A\eta}{2}) + y(2)(A + y(2))\right.\right.$$
$$\left.\left.+ \frac{\sigma_{hcnt}/\sigma_f}{\rho_{hcnt}/\rho_f} M\,y(2)\right) - 2\gamma y(3)\right] \tag{21}$$

where the energy Eq. (7) transformed as below:

$$\frac{1}{(1+2\gamma\eta)}\left[Pr\frac{(\rho c_p)_{hcnt}/(\rho c_p)_f}{K_{hcnt}/K_f}\left(-y(5)(y(1) - \frac{A\eta}{2}) + 2y(4)(A + y(2))\right.\right.$$
$$\left.\left.- \frac{\sigma_{hcnt}/\sigma_f}{(\rho c_p)_{hcnt}/(\rho c_p)_f} M\,Ec\,y(2)y(2)\right) - 2\gamma y(5)\right] \tag{22}$$

And, BC's (8) converted to:

$$ya(2) - \lambda,\ ya(1) - s,\ ya(4) - 1$$
$$yb(2),\ yb(4) \tag{23}$$

It is worth noting that a and b are corresponding to the conditions $\eta = 0$, $\eta \to \infty$ ($\eta_\infty \to 15$). The flowchart depicting of the scheme is shown as below Fig. 2.

5. Analysis and discussion

In this division, we provide an illustration to the demeanour of the flow with sundry correlated embedded factors on velocity and temperature. The transportation of heat is analysed with the leverage of Joule heating over an extended/shrunk cylinder. The duality of similarity solution can be envisioned with a precise scope of λ_c, for both shrunk and extended surface. Additionally, the demarcation of the flow is also determined (see Figs. 3–9). The numeric quantity of skin friction and Nusselt are described in tabulated data Table 3, set under various φ_2 (MWCNTs) within ϕ_1(SWCNTs) = 0.1 and $\lambda = 1$. The

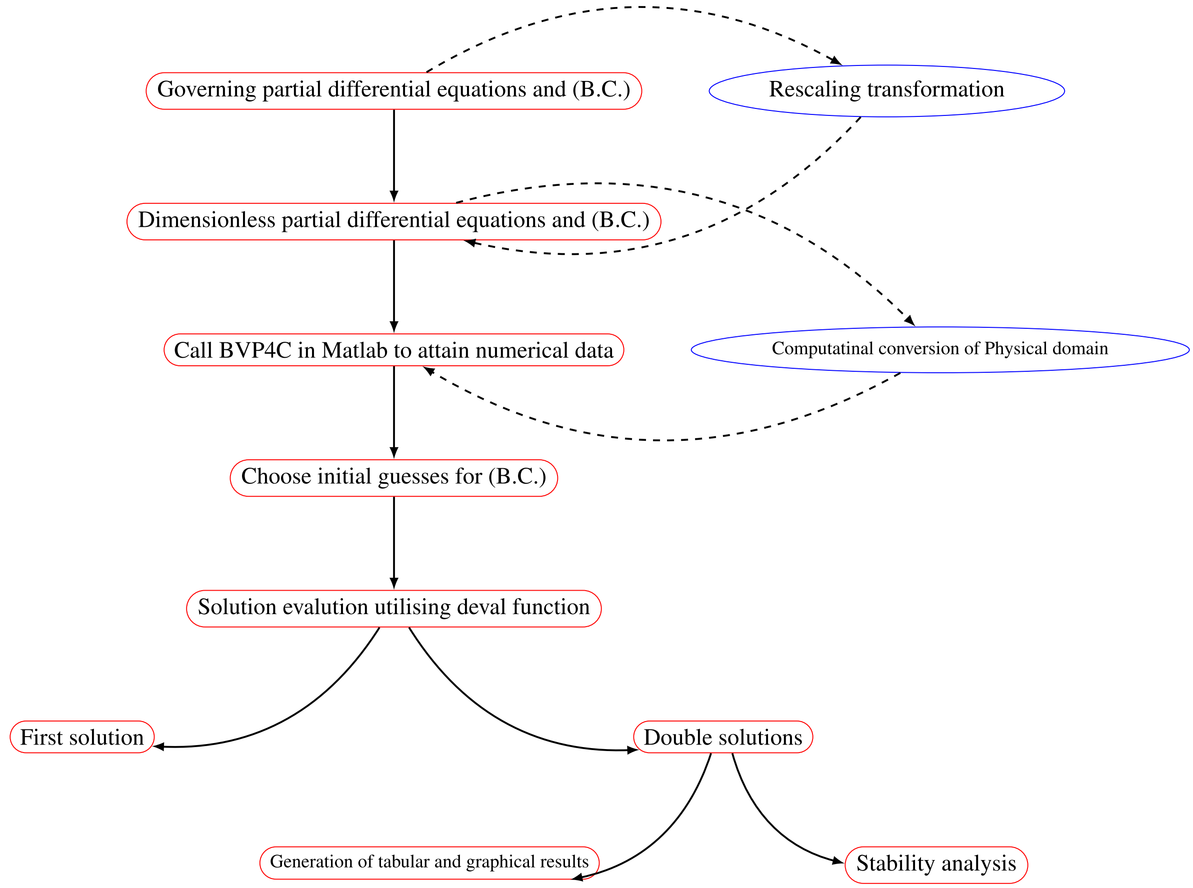

Fig. 2. Procedural flow chart of numerical methodology.

Table 3
Values of $C_f Re_x^{1/2}$ and $Nu_x Re_x^{-1/2}$ with various φ_2 when $\phi_1 = 0.1,\ S = M = \gamma = Ec = A = 0$ and $\lambda = 1$.

ϕ_2	$C_f Re_x^{1/2}$	$Nu_x Re_x^{-1/2}$
0.005	−1.2379650	5.7705356
0.02	−1.2653035	6.2724150
0.04	−1.3032590	6.8678179
0.06	−1.34304371	7.4006809

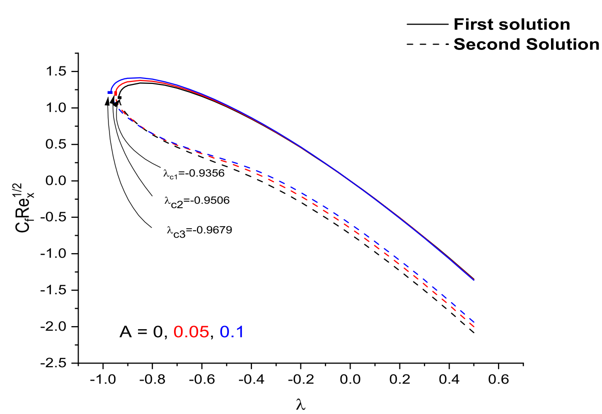

Fig. 3. Impact of A on skin friction with λ at $\gamma = 0.05, s = 2,\ \phi_2 = 0.01, Ec = M = 0.1$.

other factors is neglected. In this table, the thermophysical properties is taken as $\rho_f = 997, K_f = 0.6071, (C_p)_f = 4180$ and Pr=6.135 (see [57]). Further, the value of skin friction on extended surface deceases with the addition of ϕ_2 which implies that the surface exerts dragging on the flow. On the other hand, the heat transfer improved with the addition of ϕ_2. To assure the precision and consistency of our numerical date, the numerical date reported in Ref. [54], regenerated, which is genuinely in close alliance.

The results of the M, Ec and ϕ_2 on $f''(0)$ and $|-\theta'(0)|$ are exhibited in Table 4. The results show that the addition ϕ_2 leads to increase to $f''(0)$. The negative sign of $f''(0)$ means the stretching surface exerts a dragging force on the hybrid carbon nanotubes field. The values of heat transfer rate $|-\theta'(0)|$ have inverse relation with ϕ_2. Evidently, the addition of ϕ_2 results in a decrease in $|-\theta'(0)|$. The fluctuation in the reduced skin friction and Nusselt number for different values of γ, ϕ_1 and ϕ_2 are presented in Table 5. The value for the first solution for both of reduced skin friction and Nusselt number recorded highest value in flat surface $\gamma = 0$. Additionally, the hybrid carbon nanotubes within $\phi_1 = \phi_2 = 0.02$ has the lowest skin friction among all the listed values.

5.1. Quantities of interest in engineering concepts

Calculations and analyses of heat transfer and skin friction are considered. The Nusselt number $(Nu_x Re_x^{-1/2})$ is used to represent the rate of thermal transfer and the skin friction coefficient $(C_f Re_x^{1/2})$ is used to represent momentum travel. The default values throughout the computational process for the limiting parameters are: $M = 0.1, s = 2,\ A = 0.1, \gamma = 0.05,\ 0.01 \leqslant Ec \leqslant 0.1,\ 0.5 \leqslant \lambda \leqslant -1,\ \phi_1 = 0.1$ and $\phi_2 = 0.01$. Whereas the value of host fluid remains inflexible Pr = 6.2 (H_2O) at temperature 25°. The selection of the above values counts on suitability of numerical attainment and also from the prior studies.

Table 4
List of numerical outcomes of $f''(0)$ and $-\theta'(0)$ for various value of ϕ_2, when $\lambda = 1, s = 2, A = \phi_1 = 0.1, \gamma = 0$, and Pr $= 6.2$.

M, Ec	ϕ_2	$f''(0)$		$-\theta'(0)$	
		First solution	Second solution	First solution	Second solution
$M = 0$	0	−2.2096914	−2.6035958	5.1946161	5.1350971
$Ec = 0$	0.01	−2.1706298	−2.5570755	4.5424686	4.4777934
	0.02	−2.1318691	−2.5108445	4.0331426	3.9635040
$M = 0.1$	0	−2.2482480	−2.6288607	5.1903307	5.1332740
$Ec = 0.01$	0.01	−2.2098319	−2.5840005	4.5380126	4.4755933
	0.02	−2.1717133	−2.5394179	4.0285258	3.9608743

Table 5
List of numerical outcomes of $Re_x^{1/2}C_f$ and $Re_x^{-1/2}Nu_x$ for various value of γ, ϕ_1 and ϕ_2, for $\lambda = -1, s = 2, Ec = 0.01, A = M = 0.1$ and Pr $= 6.2$.

γ	ϕ_1	ϕ_2	$Re_x^{1/2}C_f$		$Re_x^{-1/2}Nu_x$	
			First solution	Second solution	First solution	Second solution
	0	0	1.3731311	0.7203944	10.924722	10.765505
0	0.1	0	1.4101147	1.0031581	7.0030836	4.3402862
	0	0.02	1.3458312	0.7674865	10.303311	10.041674
0.05	0	0	1.3252448	0.841313	10.897691	10.777377
	0	0.02	1.279340	0.907287	10.244722	10.068594
	0	0	1.2507003	0.9736120	10.862782	10.79246
0.1	0	0.02	1.1252135	0.9643188	10.132951	10.058145
	0.02	0	1.2373780	1.0551150	10.119441	10.022056
	0.02	0.02	1.1665949	1.1659254	9.0847753	9.1289729

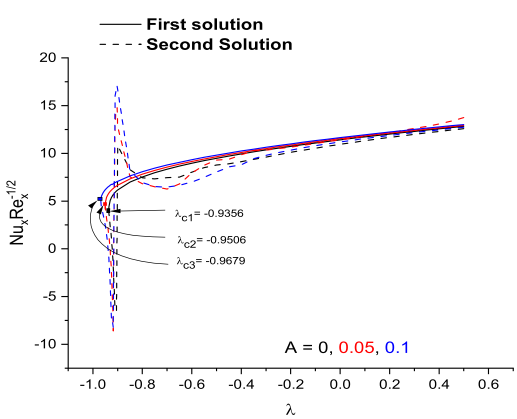

Fig. 4. Impact of A on Nusselt number with λ at $\gamma = 0.05, s = 2, \phi_2 = 0.01, Ec = M = 0.1$.

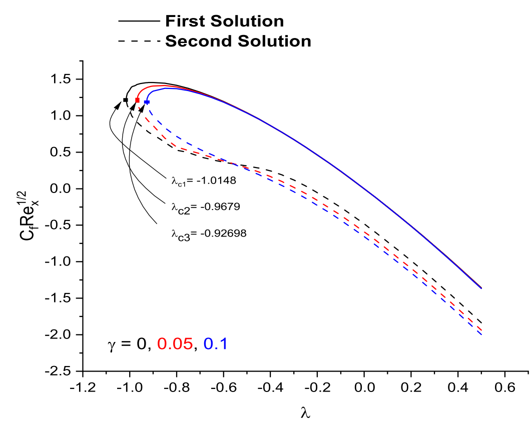

Fig. 5. Impact of γ on skin friction with λ at $A = M = 0.1, s = 2, Ec = \phi_2 = 0.01$.

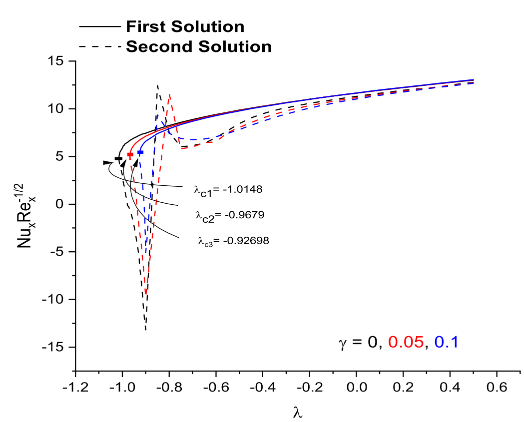

Fig. 6. Impact of γ on Nusselt number with λ at $A = M = 0.1, s = 2, Ec = \phi_2 = 0.01$.

Sketches of Figs. 3 and 4 are organized to determine how unsteady parameter (A) interacts with extended/ shrunk influence on skin friction and Nusselt number. The visualization of multiple solutions is clearly seen. Fig. 3 shows that the addition of A leads to a slight increase in skin friction value for the first solution (solid line). Subsequently, it holds up the boundary layer demarcation. Regarding the second solution (dash line), the inclination of A results in a slight detraction in the value of frictional drag. Meanwhile, Fig. 4 captured that the increment of A causes an inclination of Nusselt number for the first solution, while it shows declination for the second solution. The occurrence of this pattern is a direct consequence of extra disturbance caused by upshot the value of unsteadiness. Next, Figs. 5,Fig. 6 depict the effect of curvature γ on skin friction and thermal transfer rate. Again, visualization for multiple solutions are discernible for both assisting flow and opposing flow. The opposite demeanour is seen for the second solution. Strengthen curvature assist in speed up the detachment of the flow. Another remark is the skin dampens and Nusselt increase with an upshot of γ.

Next, Figs. 7 and 8 are prepared to illustrate the deployment of volumetric fraction of ϕHCNTs on $(C_f Re_x^{1/2})$ and $(Nu_x Re_x^{-1/2})$, within the influence of assisting/opposing flow. One of the most appealing aspects of these graphs is the growth of ϕ tends to a minor reduction in the range of solutions, leading to expedite the appearance of turbulent flow. From a physical standpoint, augmenting ϕ contribute to rise the fluid concentration and lower momentum in the boundary layer.

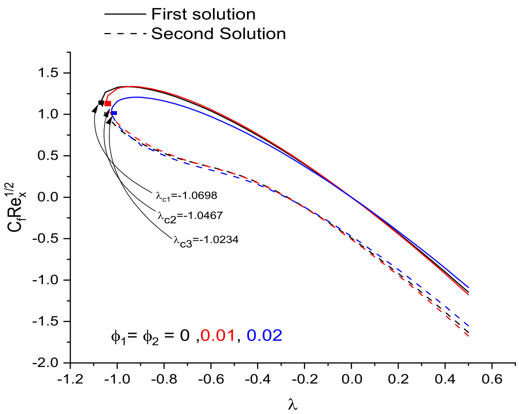

Fig. 7. Impact of ϕ on skin friction within λ at $A = M = 0.1, s = 2,\ Ec = 0.01, \gamma = 0.05$.

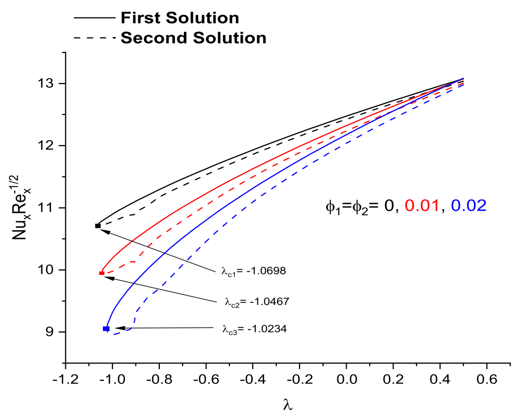

Fig. 8. Impact of ϕ on Nusselt number within λ at $A = M = 0.1, s = 2,\ Ec == 0.01, \gamma = 0.05$.

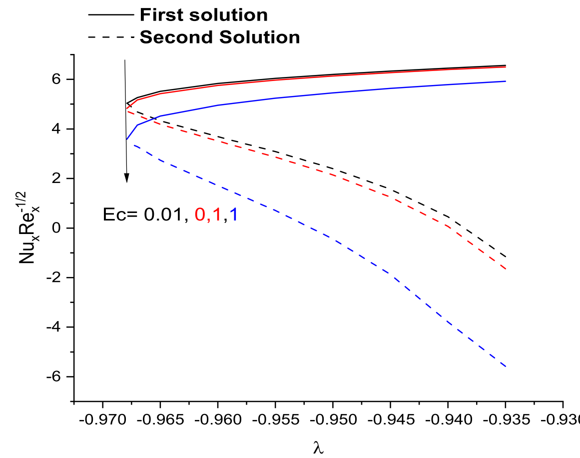

Fig. 9. Impact of Ec on Nusselt number with λ at $A = M = 0.1, s = 2, \phi_2 = 0.01, \gamma = 0.05$.

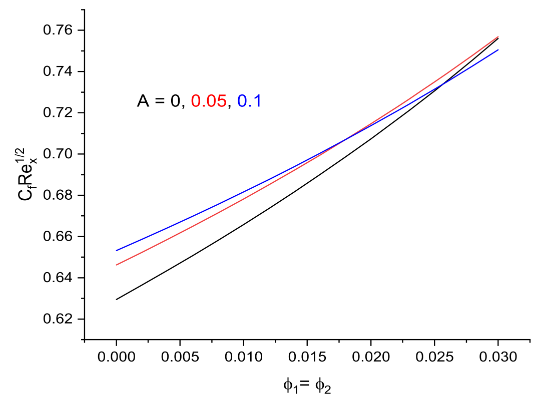

Fig. 10. Impact of A on skin friction with $\phi_1 = \phi_2$ at $\gamma = 0.05, M = 0.1, s = 2, Ec = 0.01, \lambda = -0.9$.

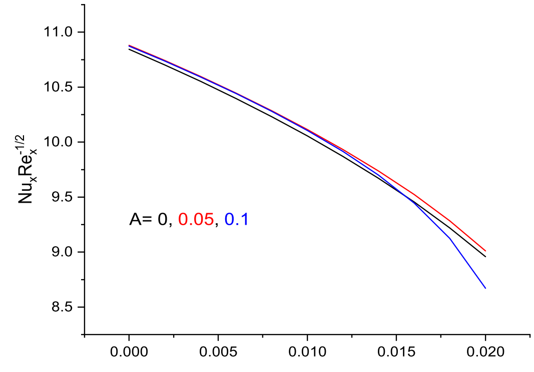

Fig. 11. Impact of A on Nusselt number with $\phi_1 = \phi_2$ at $\gamma = 0.05, M = 0.1, s = 2, Ec = 0.01, \lambda = -0.9$.

Further, the skin friction value experience an upward trend starting from assisting zone up until to the bifurcation point at opposing zone; no more solution is procured beyond these critical points. This outcome aligns with [50]. For the Nusselt number, the value experience downward trends with the addition of ϕ as viewed in Fig. 8. Clearly, the value of $(Nu_x Re_x^{-1/2})$ in assisting sector is much higher in comparison with opposing sector, this is since opposing sector hinder the travel of nanoparticle. An additional observation is that viscous fluid has highest rate of Nusselt number more than mono nanofluid (MWCNTS) and hybrid carbon nanotubes(HCNTs) as shown in Eq. (8).

Fig. 9 scrutinizes the insight of Eckert number ($Ec = 0.01, 0.1, 1$) on Nusselt number. In terms of separation flow, the fluctuations of Ec have the same peak value at the critical point in shrinking sector, which means Ec do not give any pronounced effect to alter the separation of the flow. On the other hand, the thermal boundary layer face a downward trend when Ec is upsurge. The reason for this is due to intensification of kinetic energy. These findings match up with [54].

The total composition of SWCNTs and MWCNTs volumetric fractions are implemented in a one-to-one ratio in this subdivision. For example, 1% of SWCNTs ($\phi_1 = 1\%$) as well as 1% of MWCNTs ($\phi_2 = 1\%$) are mixed to formulate 2% of SWCNTs−−MWCNTs hybrid nanoparticles volumetric fractions, donate as ϕHCNTs= 2%. The impression of a time-reliant A parameter on skin friction and Nusselt number are portrayed in Figs. 10 and 11, versus ϕHCNTs. According to the graphical sketch, the value of skin friction keeps upsurging linearly with the addition of ϕHCNTs, while the opposite behaviour can be detected from Nusselt number. Different values of unsteadiness parameter A with the addition of ϕ HCNTs contribute to a drastic drop in the value of $(Nu_x Re_x^{-1/2})$.

Figs. 12 and 13 unveils $(C_f Re_x^{1/2})$ and $(Nu_x Re_x^{-1/2})$ changes with respect to ϕHCNT, for distinct values of geometric factors γ. The value of $(C_f Re_x^{1/2})$ experience more enhancement with the addition of γ and ϕHCNTs. This means that more nanoparticles fit into cylinder with a reduction in radius, and this leads to enhancement in drag friction. As well, the value of $(Nu_x Re_x^{-1/2})$ experience a significant drop with rising strength forces provided by γ. As known, magnetic parameter play a vital role in controlling the flow. Hence, Figs. 14, Fig. 15 exclusively

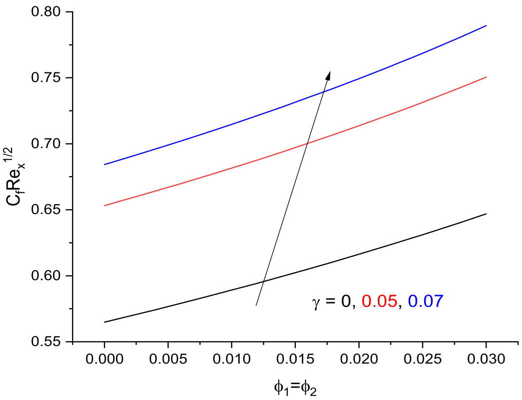

Fig. 12. Impact of γ on skin friction with $\phi_1 = \phi_2$ at $A = M = 0.1, s = 2, Ec = 0.01, \lambda = -0.9$.

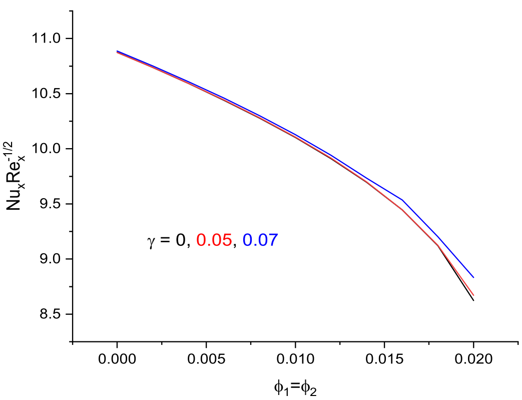

Fig. 13. Impact of γ on Nusselt number with $\phi_1 = \phi_2$ at $A = M = 0.1, s = 2, Ec = 0.01, \lambda = -0.9$.

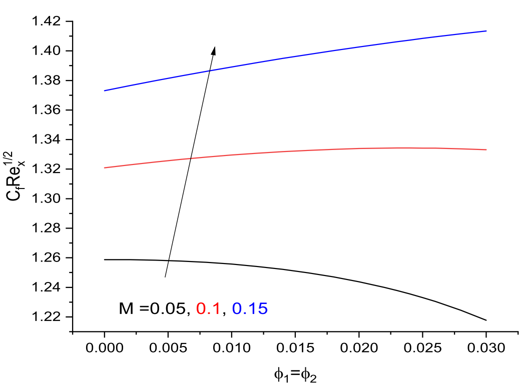

Fig. 14. Impact of M on skin friction with $\phi_1 = \phi_2$ at $\gamma = 0.05, A = M = 0.1, s = 2, Ec = 0.01, \lambda = -0.9$.

report the effect of M on skin friction and Nusselt number. In general, as M grows, the value of skin friction enhances, wherein the value of heat transfer falls dramatically with the addition of ϕHCNTs . The physical theme behind this trend is with the appearance of M, anti-flow force (Lorentz forces) is also appear which restrict fluid freedom to move and leads to minimize the velocity of hybrid carbon nanotubes. This contributes to exalts the skin friction.

5.2. Profiles of interest in physical concepts

In this section, the influences of controlling parameters on the velocity, $f'(\eta)$, and thermal allotment, $\theta(\eta)$ are highlighted to analyse

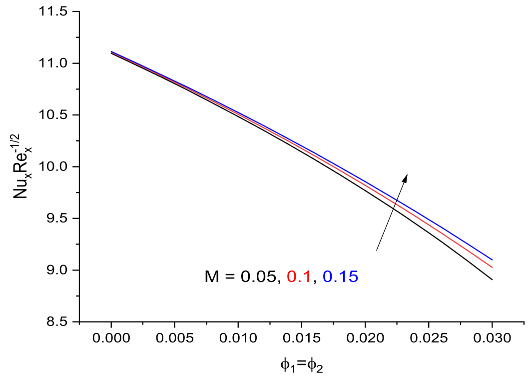

Fig. 15. Impact of M on Nusselt number with $\phi_1 = \phi_2$ at $A = M = 0.1, s = 2, Ec = 0.01, \gamma = 0.05, \lambda = -0.9$.

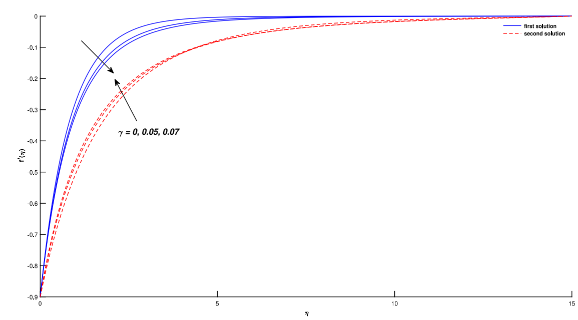

Fig. 16. Impact of γ on velocity profile at $A = M = \phi_1 = 0.1, \lambda = -0.9, s = 2, \phi_2 = Ec = 0.01$.

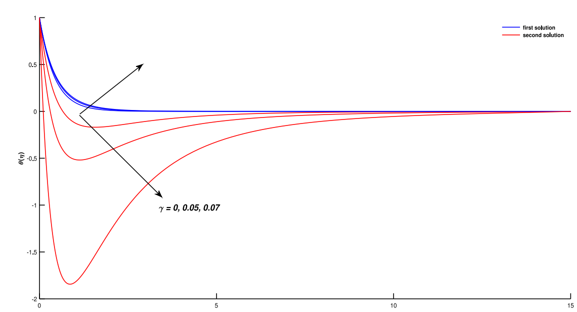

Fig. 17. Impact of γ on temperature profile at $A = M = \phi_1 = 0.1, \lambda = -0.9, s = 2, \phi_2 = Ec = 0.01$.

the boundary layer behaviour of hybrid carbon nanotubes. First and second solutions yielded and fulfilled asymptotic convergence (Eq. (8)). Figs. 16 and 17 are captured to review the presentation of γ via velocity distribution profile and thermal allotment. From this remark, the flow of velocity distribution profile declined with development of γ. Whereas, the temperature distribution steadily rising with the growth of γ for the first solution and decline for the second solution. One explanation that may be given for this trend is the cross-sectional zone trim down with upsurge γ, leading to exerted extra frictional forces on unsteady contracting cylinder. The same trend can be noticed in the fluctuation of Ec against thermal allotment. It is possible to spike up the temperature profile when Ec getting higher and higher rate across an unsteady shrinking cylinder. As can be noticed from the plot in Fig. 18. The occurrence of this rise is due to a consequence of exalts in kinetic energy which switch to thermal energy.

Sketches of Figs. 19, Fig. 20 are designed to display the effect of volumetric fraction ϕ_2 on velocity and temperature allotment. In the

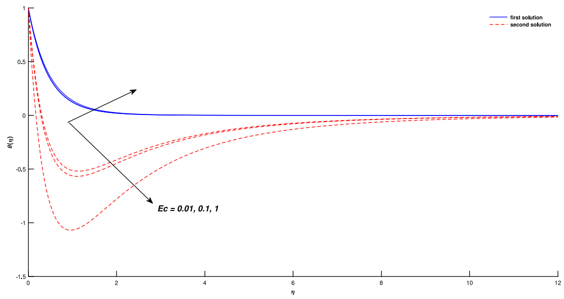

Fig. 18. Impact of Ec on temperature profile at $A = M = \phi_1 = 0.1, s = 2, \phi_2 = 0.01, \lambda = -0.9, \gamma = 0.05$.

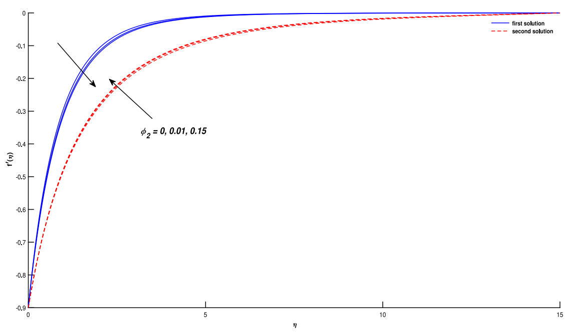

Fig. 19. Impact of ϕ_2 on velocity profile when $\lambda = -0.9, A = 0.1, s = 2, \phi_1 = 0.1, M = 0.1, Ec = 0.01$ and $\gamma = 0.05$.

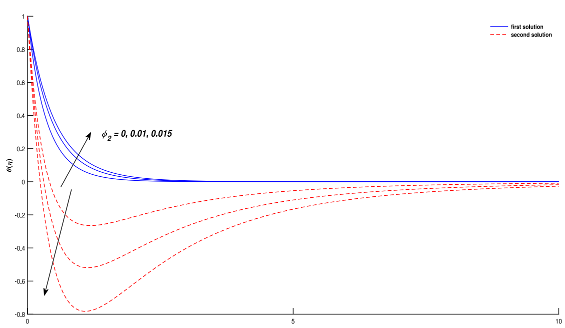

Fig. 20. Impact of ϕ_2 on temperature profile when $\lambda = -0.9, A = 0.1, s = 2, \phi_1 = 0.1, M = 0.1, Ec = 0.01/$, and $\gamma = 0.05$.

scenario of unsteady cylinder that is being shrunk. It is observed that fluid transport experience slight decelerations with an increase in ϕ_2 for all three values in the first solution. Adversely, the second solution experienced a minor acceleration. Greater ϕ_2 leads to ascending the viscosity inside hybrid carbon nanotubes, and then the resistance experience an upsurge. As a consequence, the momentum boundary layer becomes thicker and slow down. Regarding Fig. 20, thermal allotment face a slight expansion in first solution and ab opposite trend for the second solution. This outcome is identical with the study conducted by Mahabaleshwar et al. [65].

Lastly, double branches are found out in the same direction ($\lambda > 0$) and opposite direction ($\lambda < 0$). It is time now for the next step, which is to determine stability of the flow. The significance of determining stability exists in enhancing the accuracy of heat transfer process. The smallest eigenvalue α for the two emerge solutions when the variation of λ, provided that $\gamma = M = A = \phi_1 = 0.1, s = 2, Ec = 0.01$ while $\phi_2 = 0.01$ are presented in Fig. 21. Noting that, the transition value where both branches meet up is $\lambda_c = -0.92696$. After this point $\lambda < \lambda_c$ the flow will no longer satisfy the (B.C.) and will face a different flow

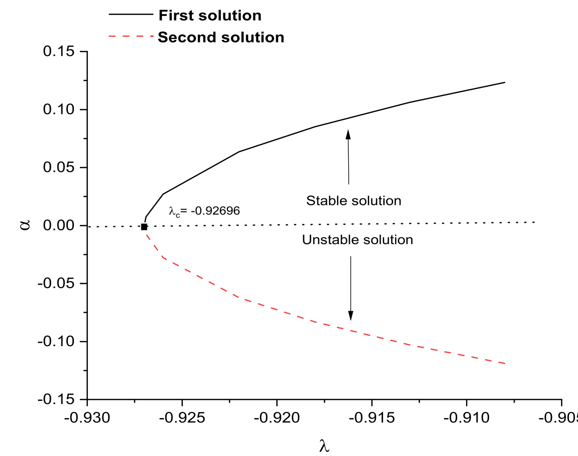

Fig. 21. Smallest eigenvalues α vs λ when $\gamma = M = A = \phi_1 = 0.1, s = 2, Ec = 0.01$ and $\phi_2 = 0.01$.

Table 6
List of several smallest eigenvalues α for different value of λ when $M = A = \phi_1 = 0.1, s = 2, Ec = 0.01$ and $\phi_2 = 0.01$.

γ	λ	α_1 First solution	α_1 Second solution
0.05	−0.95	0.4146	−0.1246
	−0.96	0.0857	−0.0835
	−0.967	0.0252	−0.0249
	−0.9676	0.0077	−0.0077
	−0.9677	0.00505	−0.0014
0.1	−0.908	0.1234	−0.119
	−0.913	0.1062	−0.1029
	−0.918	0.0852	−0.0831
	−0.922	0.0635	−0.0623
	−0.926	0.0281	−0.0278
	−0.9269	0.0076	−0.0076
	−0.92696	0.0032	−0.0032

pattern (turbulent). The outcomes of Table 6 indicates the magnitude of $(+\alpha_1) \approx 0$, $(-\alpha_2) \approx 0$ as $\lambda \to \lambda_c$. The sign of $+\alpha_1$ reflect initial decay in perturbations proving stableness (Practical) to the first branch. Conversely, the sign of $-\alpha_2$ reflect disturbance is growing, which means instability (incoherent) for second branch, as time evolves.

6. Final comments

Multiple consequences observed based on implement of various effects. The availability of double solutions is highlighted in hybrid carbon nanotubes consisting of SWCNTS–MWCNTs/water over unsteady cylinder. The impression of body forces (MHD) is accounted on the fluid momentum, while the impact of joule heating is accounted on the fluid energy. Also, the effect of stretching/shrinking and suction/injection on boundary conditions are considered. To summarized concisely;

- Augmenting unsteadiness inflates the range of solutions and retards the detachment of the boundary layer.
- By enhancing volumetric friction of ϕHCNTs and curvature, the range of solution depressed at the critical point. This accelerates the initiation of turbulence flow.
- SWCNTS–MWCNTs/H_2O with $\phi_1 = \phi_2 = 0.02$ recorded the lowest rate for skin friction and heat transfer.
- It is observed that Nusselt number experiences a notable rise with higher values of unsteadiness and an attenuation in curvature.
- Eckert Number did not show pronounced effect in regulating the detachment of the flow.
- The growth of parameters: unsteadiness A, curvature γ and MHD with the addition of ϕHCNTs shows improvement in $(C_f Re_x^{1/2})$

and declination in $(Nu_x Re_x^{-1/2})$.

- Due to elevated in curvature, Eckert number, and volumetric friction ϕ_2, velocity profile enhances.
- The profile of velocity experiences a decrease with growth in curvature and volumetric friction ϕ_2.
- Double branch solutions available in both (extending/shrinking) zones, and underscored by a stability assessment.

Finally, the generated outcome holds significant prospects for real-life application, where comprehensive insight is required to optimize the performance of diverse engineering processes. In future work, it is proposed to consider non-Newtonian flow over a vertical cylinder. In addition, it can employ sensitivity analysis (RSM).

CRediT authorship contribution statement

Dhurgham Allaw: Writing – review & editing, Writing – original draft, Software, Resources, Project administration, Methodology, Investigation, Formal analysis, Data curation, Conceptualization. **Norfifah Bachok:** Writing – review & editing, Validation, Supervision, Funding acquisition, Conceptualization. **Norihan Md Arifin:** Validation, Supervision, Conceptualization. **Fadzilah Md Ali:** Visualization, Conceptualization. **Abderrahim Wakif:** Writing – review & editing, Validation, Methodology.

Declaration of competing interest

The authors declare that they have no known competing financial interests or personal relationships that could have appeared to influence the work reported in this paper.

References

[1] S.U. Choi, J.A. Eastman, Enhancing Thermal Conductivity of Fluids with Nanoparticles, Tech. Rep., Argonne National Lab.(ANL), Argonne, IL (United States), 1995.

[2] L.J. Crane, Flow past a stretching plate, Z. Angew. Math. Phys. ZAMP 21 (1970) 645–647.

[3] C.Y. Wang, Fluid flow due to a stretching cylinder, Phys. Fluids 31 (3) (1988) 466–468.

[4] R.K. Tiwari, M.K. Das, Heat transfer augmentation in a two-sided lid-driven differentially heated square cavity utilizing nanofluids, Int. J. Heat Mass Transfer 50 (9–10) (2007) 2002–2018.

[5] J. Buongiorno, Convective transport in nanofluids, 2006.

[6] N. Bachok, A. Ishak, I. Pop, Boundary-layer flow of nanofluids over a moving surface in a flowing fluid, Int. J. Therm. Sci. 49 (9) (2010) 1663–1668.

[7] J. Merkin, N. Najib, N. Bachok, A. Ishak, I. Pop, Stagnation-point flow and heat transfer over an exponentially stretching/shrinking cylinder, J. Taiwan Inst. Chem. Eng. 74 (2017) 65–72.

[8] S. Dinarvand, R. Hosseini, M. Abulhasansari, I. Pop, Buongiorno's model for double-diffusive mixed convective stagnation-point flow of a nanofluid considering diffusiophoresis effect of binary base fluid, Adv. Powder Technol. 26 (5) (2015) 1423–1434.

[9] N. Sandeep, C. Sulochana, Dual solutions for unsteady mixed convection flow of MHD micropolar fluid over a stretching/shrinking sheet with non-uniform heat source/sink, Eng. Sci. Technol. Int. J. 18 (4) (2015) 738–745.

[10] U. Khan, N. Ahmed, S.T. Mohyud-Din, et al., Soret and dufour effects on Jeffery-Hamel flow of second-grade fluid between convergent/divergent channel with stretchable walls, Results Phys. 7 (2017) 361–372.

[11] M. Turkyilmazoglu, Radially expanding/contracting and rotating sphere with suction, Internat. J. Numer. Methods Heat Fluid Flow 32 (11) (2022) 3439–3451.

[12] N.A. Zainal, I. Waini, N.S. Khashi'ie, A.R.M. Kasim, K. Naganthran, R. Nazar, I. Pop, Stagnation point hybrid nanofluid flow past a stretching/shrinking sheet driven by Arrhenius kinetics and radiation effect, Alex. Eng. J. 68 (2023) 29–38.

[13] Z. Mahmood, S.M. Eldin, K. Rafique, U. Khan, Numerical analysis of MHD tri-hybrid nanofluid over a nonlinear stretching/shrinking sheet with heat generation/absorption and slip conditions, Alex. Eng. J. 76 (2023) 799–819.

[14] H. Alfvén, Existence of electromagnetic-hydrodynamic waves, Nature 150 (3805) (1942) 405–406.

[15] M.M. Fayyadh, K. Naganthran, M.F.M. Basir, I. Hashim, R. Roslan, Radiative MHD sutterby nanofluid flow past a moving sheet: Scaling group analysis, Mathematics 8 (9) (2020) 1430.

[16] Z. Mahmood, S.E. Alhazmi, A. Alhowaity, R. Marzouki, N. Al-Ansari, U. Khan, MHD mixed convective stagnation point flow of nanofluid past a permeable stretching sheet with nanoparticles aggregation and thermal stratification, Sci. Rep. 12 (1) (2022) 16020.

[17] U. Mahabaleshwar, T. Anusha, S. Sachhin, D. Zeidan, S.W. Joo, An impact of richardson number on the inclined MHD mixed convective flow with heat and mass transfer, Heat Transf. 53 (6) (2024) 3104–3124.

[18] A.M. Soomro, M.A. Fadhel, L.A. Lund, Z. Shah, M.H. Alshehri, N. Vrinceanu, Dual solutions of magnetized radiative flow of casson nanofluid over a stretching/shrinking cylinder: Stability analysis, Heliyon (2024) e29696.

[19] N. Abbas, W. Shatanawi, K. Abodayeh, T.A. Shatnawi, Comparative analysis of unsteady flow of induced MHD radiative sutterby fluid flow at nonlinear stretching cylinder/sheet: Variable thermal conductivity, Alex. Eng. J. 72 (2023) 451–461.

[20] J. Wang, N.A. Shah, B. Almutairi, O.K. Kwon, J.D. Chung, Bvp4c approach and duality of hybrid nanofluid over extending and contracting sheet with chemical reaction and cross-diffusion effects, Results Phys. 57 (2024) 107362.

[21] Y. Bai, H. Yue, R. Zhang, W. Qian, Z. Zhang, F. Wei, Mechanical behavior of single and bundled defect-free carbon nanotubes, Accounts Mater. Res. 2 (11) (2021) 998–1009.

[22] S. Beg, M. Rizwan, A.M. Sheikh, M.S. Hasnain, K. Anwer, K. Kohli, Advancement in carbon nanotubes: basics, biomedical applications and toxicity, J. Pharm. Pharmacol. 63 (2) (2011) 141–163.

[23] M. Ovais, M. You, J. Ahmad, R. Djellabi, A. Ali, M.H. Akhtar, M. Abbas, C. Chen, Engineering carbon nanotubes for sensitive viral detection, TRAC Trends Anal. Chem. 153 (2022) 116659.

[24] R.H. Baughman, A.A. Zakhidov, W.A. De Heer, Carbon nanotubes–the route toward applications, Science 297 (5582) (2002) 787–792.

[25] M.F. De Volder, S.H. Tawfick, R.H. Baughman, A.J. Hart, Carbon nanotubes: present and future commercial applications, Science 339 (6119) (2013) 535–539.

[26] Y. Al-Douri, Graphene, Nanotubes and Quantum Dots-Based Nanotechnology: Fundamentals and Applications, Woodhead Publishing, 2022.

[27] S. Rathinavel, K. Priyadharshini, D. Panda, A review on carbon nanotube: An overview of synthesis, properties, functionalization, characterization, and the application, Mater. Sci. Eng. B 268 (2021) 115095.

[28] S. Iijima, Helical microtubules of graphitic carbon, Nature 354 (6348) (1991) 56–58.

[29] S. Iijima, T. Ichihashi, Single-shell carbon nanotubes of 1-nm diameter, Nature 363 (6430) (1993) 603–605.

[30] M. Waqas, T. Hayat, A. Alsaedi, A theoretical analysis of SWCNT–MWCNT and H 2 O nanofluids considering Darcy–Forchheimer relation, Appl. Nanosci. 9 (2019) 1183–1191.

[31] M. Gholinia, M. Armin, A. Ranjbar, D. Ganji, Numerical thermal study on CNTs/C2H6O2–H2O hybrid base nanofluid upon a porous stretching cylinder under impact of magnetic source, Case Stud. Therm. Eng. 14 (2019) 100490.

[32] K. Muhammad, T. Hayat, A. Alsaedi, B. Ahmed, A comparative study for convective flow of basefluid (gasoline oil), nanomaterial (SWCNTs) and hybrid nanomaterial (SWCNTs+ MWCNTs), Appl. Nanosci. 11 (2021) 9–20.

[33] M. Hussain, M. Sheremet, Convective-radiative magnetized dissipative nanofluid (CNTs-water) transport in porous media, using Darcy–Brinkman–Forchheimer model, Int. Commun. Heat Mass Transfer 139 (2022) 106420.

[34] F.Z. Duraihem, E. Maraj, N.S. Akbar, R. Mehmood, Thermal stratification effect on gravity driven transport of hybrid CNTs down a stretched surface through porous medium, Heliyon 9 (5) (2023).

[35] G.K. Ramesh, J. Madhukesh, N.A. Shah, S.-J. Yook, Flow of hybrid CNTs past a rotating sphere subjected to thermal radiation and thermophoretic particle deposition, Alex. Eng. J. 64 (2023) 969–979.

[36] K. Rafique, Z. Mahmood, U. Khan, S.M. Eldin, A.M. Alzubaidi, Mathematical analysis of radius and length of CNTs on flow of nanofluid over surface with variable viscosity and joule heating, Heliyon 9 (7) (2023).

[37] R. Tabassum, A. Al-Zubaidi, S. Rana, R. Mehmood, S. Saleem, Slanting transport of hybrid (MWCNTs-SWCNTs/H2O) nanofluid upon a Riga plate with temperature dependent viscosity and thermal jump condition, Int. Commun. Heat Mass Transfer 135 (2022) 106165.

[38] S.N.A. Salleh, N.A.M. Zin, N. Najib, Verification of dual solutions for water and kerosene-based carbon nanotubes over a moving slender needle, Symmetry 14 (11) (2022) 2306.

[39] R. Mahesh, U. Mahabaleshwar, E.H. Aly, O. Manca, An impact of CNTs on an MHD Casson Marangoni boundary layer flow over a porous medium with suction/injection and thermal radiation, Int. Commun. Heat Mass Transfer 141 (2023) 106561.

[40] H. Ali Ghazwani, M. Saleem, F. Haq, Magnetized radiative flow of propylene glycol with carbon nanotubes and activation energy, Sci. Rep. 13 (1) (2023) 21813.

[41] W. Khan, T. Yusuf, F. Mabood, M. Siddiq, S. Shehzad, Chemically reactive water-based carbon nanotubes flow saturated in Darcy-Forchheimer porous media coupled with entropy generation, Chem. Phys. Lett. 830 (2023) 140808.

[42] N.A.A. Samat, N. Bachok, N.M. Arifin, Magnetohydrodynamic flow of carbon nanotubes and heat transfer over a moving thin needle: A numerical and research surface methodology, Ain Shams Eng. J. (2024) 102833.

[43] N. Riley, Unsteady laminar boundary layers, SIAM Rev. 17 (2) (1975) 274–297.
[44] D.P. Telionis, D.P. Telionis, Unsteady Viscous Flows, vol. 320, Springer, 1981.
[45] K. Bhattacharyya, Heat transfer analysis in unsteady boundary layer stagnation-point flow towards a shrinking/stretching sheet, Ain Shams Eng. J. 4 (2) (2013) 259–264.
[46] M.V. Krishna, A.J. Chamkha, Hall and ion slip effects on MHD rotating boundary layer flow of nanofluid past an infinite vertical plate embedded in a porous medium, Results Phys. 15 (2019) 102652.
[47] M.V. Krishna, A.J. Chamkha, Hall and ion slip effects on MHD rotating flow of elastico-viscous fluid through porous medium, Int. Commun. Heat Mass Transfer 113 (2020) 104494.
[48] M.V. Krishna, N.A. Ahamad, A.J. Chamkha, Hall and ion slip effects on unsteady MHD free convective rotating flow through a saturated porous medium over an exponential accelerated plate, Alex. Eng. J. 59 (2) (2020) 565–577.
[49] S. Suganya, M. Muthtamilselvan, F. Al-Amri, B. Abdalla, D.-H. Doh, Filtration of radiating and reacting SWCNT–MWCNT/water hybrid flow with the significance of Darcy–Forchheimer porous medium, Arab. J. Sci. Eng. 46 (2021) 1981–1995.
[50] D. Allaw, N. Bachok, N.M. Arifin, F.M. Ali, Double solutions of unsteady stagnation-point of carbon nanotubes across a permeable exponential stretching/shrinking sheet, Chinese J. Phys. 85 (2023) 534–552.
[51] U. Mahabaleshwar, K. Sneha, L. Pérez, O. Manca, An unsteady flow through porous media leads to a Newtonian fluid presence of CNTS and suction/injection, Int. Commun. Heat Mass Transfer 145 (2023) 106844.
[52] A. Tulu, L. Asefa, M. Sohail, Unsteady magnetohydrodynamic hybrid nanofluid flow over a rotating disk with viscous dissipation and Cattaneo–Christov heat flux model, Int. J. Thermofluids (2024) 100586.
[53] Q. Xue, Model for thermal conductivity of carbon nanotube-based composites, Phys. B 368 (1–4) (2005) 302–307.
[54] N.S. Khashi'ie, N.M. Arifin, I. Pop, N.S. Wahid, Flow and heat transfer of hybrid nanofluid over a permeable shrinking cylinder with Joule heating: a comparative analysis, Alex. Eng. J. 59 (3) (2020) 1787–1798.
[55] I. Waini, A. Ishak, I. Pop, Unsteady flow and heat transfer past a stretching/shrinking sheet in a hybrid nanofluid, Int. J. Heat Mass Transfer 136 (2019) 288–297.
[56] D. Allaw, N. Bachok, N.M. Arifin, F.M. Ali, The boundary layers of an unsteady stagnation points flow in carbon nanotubes, J. Adv. Res. Fluid Mech. Therm. Sci. 75 (1) (2020) 12–20.
[57] S.S.U. Devi, S.A. Devi, Numerical investigation of three-dimensional hybrid Cu–Al2O3/water nanofluid flow over a stretching sheet with effecting Lorentz force subject to Newtonian heating, Can. J. Phys. 94 (5) (2016) 490–496.
[58] Y. Lin, S. Rehman, N. Akkurt, T. Shedd, M. Kamran, M.I. Qureshi, T. Botmart, A.N. Alharbi, A. Farooq, I. Khan, Free convective trickling over a porous medium of fractional nanofluid with MHD and heat source/sink, Sci. Rep. 12 (1) (2022) 20778.
[59] W. Khan, Z. Khan, M. Rahi, Fluid flow and heat transfer of carbon nanotubes along a flat plate with Navier slip boundary, Appl. Nanosci. 4 (2014) 633–641.
[60] U. Mahabaleshwar, S. Sachin, A. Vishalakshi, G. Bognar, B.A. Sunden, Linear stability analysis of micropolar nanofluid flow across the accelerated surface with inclined magnetic field, Internat. J. Numer. Methods Heat Fluid Flow 34 (9) (2024) 3515–3541.
[61] J. Merkin, On dual solutions occurring in mixed convection in a porous medium, J. Engrg. Math. 20 (2) (1986) 171–179.
[62] P. Weidman, D. Kubitschek, A. Davis, The effect of transpiration on self-similar boundary layer flow over moving surfaces, Internat. J. Engrg. Sci. 44 (11–12) (2006) 730–737.
[63] S. Harris, D. Ingham, I. Pop, Mixed convection boundary-layer flow near the stagnation point on a vertical surface in a porous medium: Brinkman model with slip, Transp. Porous Media 77 (2009) 267–285.
[64] L.F. Shampine, I. Gladwell, S. Thompson, Solving ODEs with Matlab, Cambridge University Press, 2003.
[65] U. Mahabaleshwar, K. Sneha, A. Chan, D. Zeidan, An effect of MHD fluid flow heat transfer using CNTs with thermal radiation and heat source/sink across a stretching/shrinking sheet, Int. Commun. Heat Mass Transfer 135 (2022) 106080.